International Journal of Automotive Technology, Vol. 4, No. 2, pp. 87–94 (2003)

1229–9138/2003/012–04

MODELING OF IRON LOSSES IN PERMANENT MAGNET SYNCHRONOUS MOTORS WITH FIELD-WEAKENING CAPABILITY FOR ELECTRIC VEHICLES

Y.-K. CHIN* and J. SOULARD

Royal Institute of Technology (KTH), Competence Center in Electric Power Engineering, Permanent Magnet Drives (PMD) Research Group, Teknikringen 33, Stockholm 10044, Sweden

(Received 8 October 2002; Revised 11 March 2003)

ABSTRACT–Recent advancements of permanent magnet (PM) materials and solid-state devices have contributed to a substantial performance improvement of permanent magnet machines. Owing to the rare-earth PMs, these motors have higher efficiency, power factor, output power per mass and volume, and better dynamic performance than induction motors without sacrificing reliability. Not surprisingly, they are continuously receiving serious considerations for a variety of automotive and propulsion applications. An electric vehicle (EV) requires a high-efficient propulsion system having a wide operating range and a capability of generating a high peak torque for short durations. The improvement of torque-speed performance for these systems is consequently very important, and researches in various aspects are therefore being actively pursued. A great emphasis has been placed on the efficiency and optimal utilization of PM machines. This requires attention to many aspects related to the machine design and overall performance. In this respect, the prediction of iron losses is particularly indispensable and challenging, especially for drives with a deep field-weakening range. The objective of this paper is to present iron loss estimations of a PM motor over a wide speed range. As aforementioned, in EV applications core losses can be significant during high-speed operation and it is imperative to evaluate these losses accurately and take them into consideration during the motor design stage. In this investigation, the losses are predicted by using an analytical model and a 2D time-stepped finite element method (FEM). The results from different analytical approaches are compared with the FEM computations. The validity of each model is then evaluated by these comparisons.

KEY WORDS : Efficiency, Electric drive, EV, Modeling, Permanent magnet motor, Power density

NOMENCLATURE

B_{tm} = maximum teeth flux density
B_{ym} = maximum yoke flux density
B_m = maximum air gap flux density
B_{arm} = amplitude of the armature flux density
- d = parameters in d-axis
- q = parameters in q-axis
V_t = teeth volume in m^3
V_y = yoke volume in m^3
p = machine pole number
Y = current angle
b_{ts} = width of the teeth = α_{tt}
h_{ss} = stator back height or yoke height
β_m = magnet span in electrical radians = 2α
Φ_m = magnet flux
Φ_T = resultant air gap flux
Φ_F = field weakening flux
Φ_a = armature flux
Φ_S = resultant flux
σ_t = skew angle
k_h = hysteresis loss constant
k_e = eddy current loss constant
k_{exc} = excess loss constant
k_{ch} = correction factor for minor hysteresis loops
n = Steinmetz constant
r = air gap radius
τ_s = slot pitch
τ_p = pole pitch
ω = frequency in radians per second
ω_s = synchronous frequency/speed
ω_b = base frequency
q = number of slot per pole per phase

**Corresponding author.* e-mail: robert.chin@ekc.kth.se

1. INTRODUCTION

Since the introduction of Neodymium-iron-boron (Nd-Fe-B) magnet materials in late 1983, as it was outlined by Sagawa *et al.* (1984), vast amount of attention has been

given to the application of these materials in permanent magnet (PM) motors. Gieras (1997) also mentioned that these PM motors tend to replace induction motors in various applications as they present higher efficiency, power factor and specific output power. For a given frame size, a conventional radial surface mounted PM motor, as depicted in Figure 1(a), can produce a subsequently larger steady-state torque than obtainable from an induction motor. It has also been shown by Sebastian & Slemon (1987) that these PM motors can be operated over a considerably extended speed range at near-constant power through control of the angle between the stator and rotor field. Not surprisingly, a great emphasis has been placed on the efficiency and the optimal utilisation of PM motors for a variety of automotive applications. The iron losses can account for a significant portion of the total loss in a PM motor, particularly when it operates above the rated speed in the field-weakening region. The output power capability of PM motors at higher speed is strongly limited by the increase of iron loss. In order to reach the desired performance throughout the whole speed range, these losses should be carefully studied as a part of the design considerations.

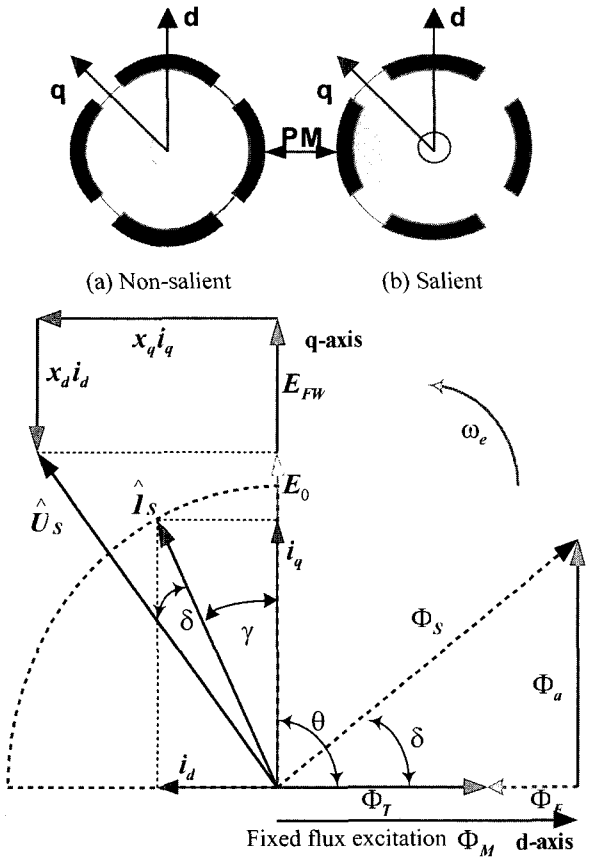

(c) PM motor phasor diagram

Figure 1. Rotor configurations of PM motors: (a) Surface Mounted PM (SMPM); (b) Surface Inset PM (IPM); (c) Phasor diagram showing field-weakening operation.

2. LITERATURE REVIEW ON PREVIOUS STUDIES

Iron losses in electrical machines are usually predicted by assuming that the magnetic flux in the magnetic core has only one alternating component that is sinusoidal. According to the conventional Steinmetz model, when a piece of core material is subjected to a sinusoidal flux density of varying amplitude and frequency, the core loss density (in W/kg or W/m^3) is given as:

$$P_{core} = P_h + P_{eddy} = k_h f \hat{B}^n + k_e f^2 \hat{B}^2 \qquad [\mathrm{W/m^3}] \quad (1)$$

Berotti *et al.* (1991) pointed out that iron losses evaluated by this approach may be 20% lower than the measured values and discrepancy is even larger in PM machines. This is mainly due to the non-sinusoidal flux density waveform in critical regions of PM motors. The fact that the flux density variation is not sinusoidal greatly influences the eddy current losses, as the induced circulating current is a function of *dB/dt*. An alternative approach by Jamil & Demerdash (1990) considers the harmonics of the magnetic flux density and the sum of losses from each component gives the total core losses. This method requires high effort and is time consuming (with FEM) as the precise calculation of electromagnetic fields is needed. Nevertheless, a good estimation can be achieved with this approach.

An analytical model, developed by Slemon & Liu (1990), uses a simple approach to estimate the no-load iron losses in PM synchronous motors. It was assumed in their study that: i) the tooth and yoke flux waveforms are trapezoidal with regard to time; ii) eddy current loss is proportional to the square of time rate of the magnitude of flux density. The overall application of these approximations produced an acceptable prediction of the total measured iron losses in an experimental machine. The model derived by them is as follows:

$$P_{core} = P_h + P_{eddy} = k_h \omega \cdot [V_t \hat{B}_t^n + V_y \hat{B}_y^n] + \frac{4}{\pi} k_h \omega^2 \left[\frac{2r}{p b_{ts}} V_t \hat{B}_t^2 + \frac{V_y \hat{B}_y^2}{\alpha} \right] \qquad [\mathrm{W}] \quad (2)$$

Deng (1999) evaluated the no load iron losses in a SMPM motor in a similar procedure proposed by Slemon & Liu (1990). In addition, the approach also accounts for excess or anomalous losses, the eddy current loss is expressed in term of *RMS* value of *dB/dt*. A general expression that includes the harmonic effect on the core losses is then written as follows:

$$P_t=P_h+P_e+P_{exc}=k_{ch}k_h f\cdot \hat{B}_m^n + \frac{k_e}{2\pi^2}\left(\frac{dB}{dt}\right)_{rms}^2+\frac{k_{exc}}{(2\pi^2)^{0.75}}\left(\frac{dB}{dt}\right)_{rms}^{3/2} \quad [W/M^3] \quad (3)$$

The expression is evaluated further by deriving *dB/dt* analytically as:

$$P_t=\left\{\begin{array}{c}\left[k_h f\cdot B_{tm}^n+\frac{4}{\pi(\alpha_{tt}+\sigma_t)}\frac{f^2B_{tm}^2k_e}{}\right]+\\ \left[\frac{4}{\pi(\alpha_{tt}+\sigma_t)}\frac{k_{exc}}{}\right]^{3/4} f^{1.5}B_{tm}^{1.5}\end{array}\right\}\cdot V_t$$

$$+\left\{\begin{array}{c}\left[k_h f\cdot B_{ym}^n+\frac{8}{\pi\ \beta_m}\frac{f^2B_{ym}^2k_e}{}\right]+\\ \left(\frac{8}{\pi\ \beta_m}\frac{k_{exc}}{}\right)^{3/4} f^{1.5}B_{tm}^{1.5}\end{array}\right\}\cdot V_y \quad [W/m^3] \quad (4)$$

However, the geometric effects are also neglected and only the magnitude of the magnetic flux density is used to perform the calculation. Mi, Slemon & Bonert (2001) have most recently presented a simplified model to calculate the no load core losses. In their study, correction factors are introduced to reflect the geometrical influences and effect of the circumferential component of the tooth flux density. The expressions proposed are as follow:

Hysteresis Losses;

$$P_h=k_h\omega B_t^n+k_h\omega B_y^n \quad [W/m^3] \quad (5)$$

Eddy Current Losses;

$$P_e=\frac{12}{\pi^2}qk_qk_ck_e(\omega\cdot B_t)^2+\frac{1}{\alpha}\frac{8}{\pi^2}k_ek_r\omega^2\hat{B}_y^2 \quad [W/m^3] \quad (6)$$

In addition to the all above, Lavers *et al.* (1978) introduce an empirical correction factor, k_{ch}, to account for the effect of minor hysteresis loops on the hysteresis loss. Minor hysteresis loops are due to the small flux variations that are caused by the slotting of the stator geometry, as illustrated in Figure 2, k_{ch} is defined as

$$k_{ch}=1+\frac{c}{B_m}\sum_{i=1}^{N}\Delta B_i \quad (7)$$

where B_m is the peak value of the flux density; ΔB_i is the flux variation around the minor loop and c is a constant from 0.6 to 0.7. Model I in our study is based on expressions (4)~(6), the no-load core loss equivalent resistance is then calculated for the d- and q- equivalent circuit. As it can be noticed, all above-mentioned

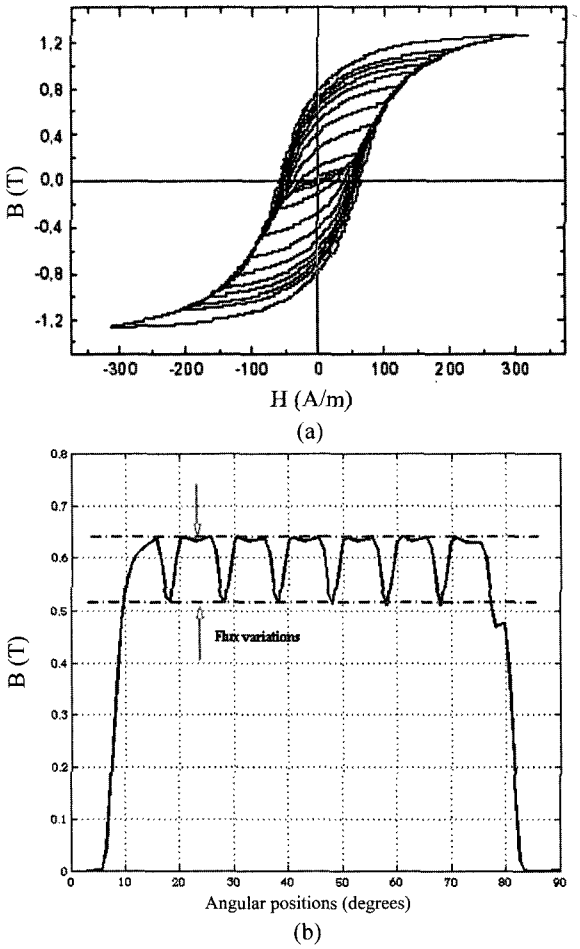

Figure 2. (a) Minor hysteresis loops, (b) Flux density variations in the air gap.

expressions are derived based on the no-load condition, *i.e. no stator armature flux linkage. Model II is developed* by accounting the effect of the load current on the air gap flux density waveform.

3. MODEL I: SIMPLE CORE LOSSES MODEL BASED ON THE NO-LOAD IRON LOSSES

A widely used equivalent circuit of a PM motor based on a synchronous d-q reference frame is presented in Figure 3. The effect of the iron losses is modeled by placing a parallel core resistance in both d- and q- equivalent model. The steady state equations can be written as

$$\begin{pmatrix}u_d\\u_q\end{pmatrix}=\begin{pmatrix}R_s & -\omega_s L_q\\ \omega_s\cdot L_d & R_s\end{pmatrix}\cdot\begin{pmatrix}i_d\\i_q\end{pmatrix}+\begin{pmatrix}0\\ \omega\cdot\Phi_a\end{pmatrix} \quad (8)$$

Neglecting the stator resistance, the no load iron losses P_{fe} are given by

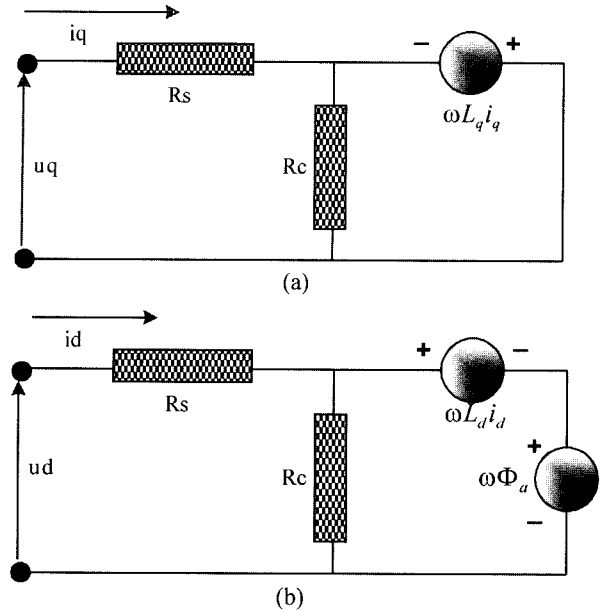

Figure 3. Equivalent circuit for PM motors including iron losses: (a) d-axis; (b) q-axis.

$$P_{fe}=\frac{u^2}{R_c}=\frac{u_d^2+u_q^2}{R_c}\frac{\omega^2}{R_c}\cdot[(\Phi_M+L_d i_d)^2+(L_q\cdot i_q)^2] \tag{9}$$

The value of the resistance can be modelled as a function of the operating frequency and the no-load core resistance R_{co}. The core resistance R_c is divided into three parallel resistances for hysteresis losses, eddy current losses and excess losses respectively. The hysteresis losses resistance R_{ch} is proportional to the frequency and the eddy current resistance R_{ce} does not depend on the frequency. With the same argument, the excess losses resistance R_{cexc} are also derived. Their expressions are

$$R_{ch}=R_{ch0}\cdot\left(\frac{\omega}{\omega_b}\right) \tag{10}$$

$$R_{ce}=R_{ce0} \tag{11}$$

$$R_{cexc}=R_{cexc0}\cdot\left(\frac{\omega}{\omega_b}\right)^{0.5} \tag{12}$$

where R_{h0}, R_{e0}, R_{exc0} are calculated at no-load condition at the rated operating frequency. They are calculated as

$$R_{ch0}=\frac{u_{rated}^2}{P_{hys0}} \tag{13}$$

$$R_{ce0}=\frac{u_{rated}^2}{P_{eddy0}} \tag{14}$$

$$R_{cexc0}=\frac{u_{rated}^2}{P_{exc0}} \tag{15}$$

In this study, the analytical approaches proposed by *MI*

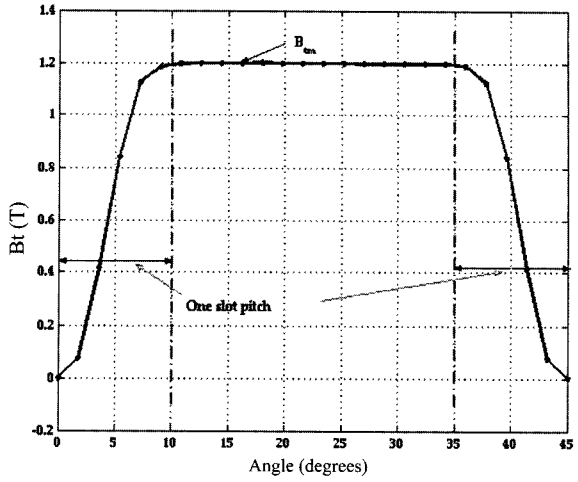

(a) Raidal tooth flux density

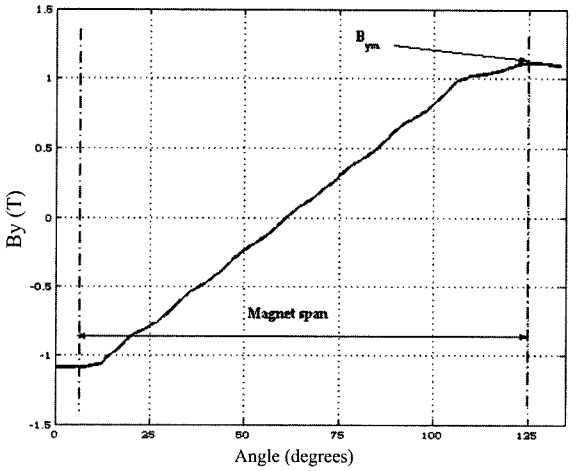

(b) Tangential yoke flux density

Figure 4. FEM approximation of the flux density rise time in: (a) Teeth; (b) Yoke, respectively.

ET AL. and *Deng* are used to calculate the no-load losses at rated condition. It has been found that the calculated loss is almost twice of that calculated by FEM if the rise time of the tooth flux density is assumed to be a tooth width. However, it has been shown that the estimation is close (with 5%) to the FEM calculation when the rise time of the tooth flux density, as shown in Figure 4(a), is assumed to be approximately one slot pitch. This is also further agreed by *Mi's* investigation. Equation (4) can then be modified by replacing α_{tt} with τ_s. The corrected equation is as follow:

$$P_t=\left\{\begin{array}{c}\left[k_h f\cdot B_{tm}^n+\dfrac{4}{\pi}\dfrac{f^2B_{tm}^2k_e}{(\alpha_{tt}+\sigma_t)}\right]+\\ \left[\dfrac{4}{\pi}\dfrac{k_{exc}}{(\tau_s+\sigma_t)}\right]^{3/4}f^{1.5}B_{tm}^{1.5}\end{array}\right\}\cdot V_t$$

$$+\left\{\left[k_h f\cdot B_{ym}^{n}+\frac{8f^2B_{ym}^2k_e}{\pi\ \beta_m}\right]+\left(\frac{8}{\pi}\frac{k_{exc}}{\beta_m}\right)^{3/4}f^{1.5}B_{tm}^{1.5}\right\}\cdot V_y \qquad [\mathrm{W/m^3}]\ (16)$$

4. MODEL II: ANALYTICAL APPROACH BASED ON TEETH AND YOKE FLUX DENSITY WAVEFORMS

In this section, an analytical model that accounts the stator armature reaction is described. Figure 5 illustrates the air gap flux density waveform and its two components, the magnet flux density B_m and the armature current flux density B_{arm}. The magnet flux density waveform can be approximated by a trapezoidal waveform or a sinusoidal wave at the fundamental frequency. The flux density waveforms in the teeth and yoke can be derived respectively from the resultant flux density in the air gap. For the teeth flux density, it is assumed that all the air gap fluxes over one slot pitch τ_s passes through the corresponding the stator tooth without any leakage. It is also suggested that the radial component of the teeth flux is the prominent one, tangential components are very small and can be neglected. The flux density in the teeth can be obtained as:

$$B_t(\theta)=\left(\frac{1}{b_{ts}}\right)\cdot\int_{\theta}^{\theta+\tau_s}[B_m(\theta)+\hat{B}_{arm}\cdot\cos(\theta+\gamma)]\cdot r\cdot d\theta \qquad (17)$$

In contrary, the main component of the flux in the yoke (stator back) is in the tangential direction. This might not be completely true in the yoke region from the teeth projection, where there might be some influential radial flux. As depicted in Figure 6, it can be noted that the flux in the radial direction is decaying rapidly towards the peripheral of the yoke. The gradient of the decreasing radial flux density can be approximated as:

$$B_{teeth\_projection\_r}(\theta)=\frac{B_t(\theta)}{\sqrt{7}} \qquad (18)$$

These radial components of the flux might only contribute a very minor portion of the total flux and become negligible in the rest of the yoke region. Nevertheless, it

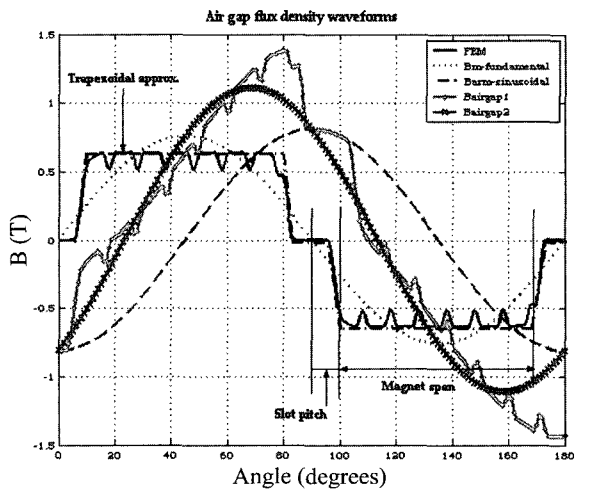

Figure 5. Air gap flux density waveform: i) Magnet flux density waveform B_m (FEM); ii) Armature current flux density waveform B_{arm}; iii) Fundamental of B_m; iv) Trapezoidal approximation.

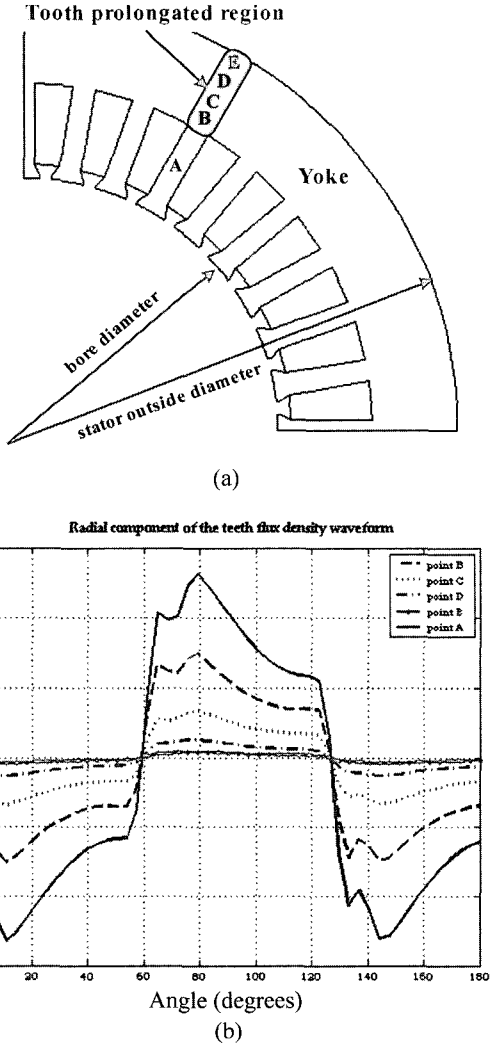

Figure 6. The radial component of the teeth flux: (a) a section of the stator geometry with the teeth projection area in the yoke; (b) flux densities at various points, A, B, C, D and E.

might be essential to consider it when the flux is highly distorted in deep flux weakening region. For the tangential flux density in the yoke, it is assumed that the total air gap flux over one pole pitch τ_p splits into two and complete the path through to the adjacent pole respectively. The flux density waveforms in the yoke can then be derived as

$$B_y(\theta)=\left(\frac{1}{2\cdot h_{ss}}\right)\cdot\int_{\theta}^{\theta+\tau_p}[B_m(\theta)+\hat{B}_{arm}\cdot\cos(\theta+\gamma)]\cdot r\cdot d\theta \tag{19}$$

As aforementioned, two approximations are used to describe $B_m(\theta)$: sinusoidal and trapezoidal waveforms. Figure 7(a) and Figure 7(b) shows the obtained analytical teeth and yoke waveforms from the two approaches respectively. The losses in the teeth and yoke

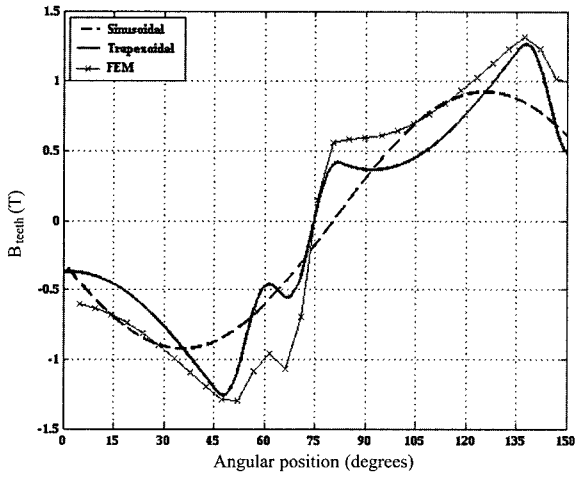

(a) Teeth

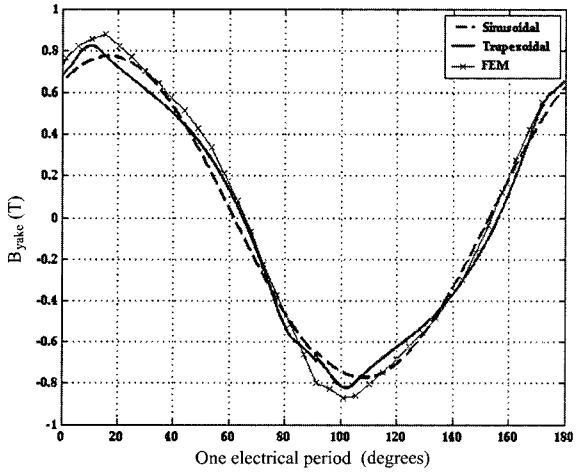

(b) Yoke

Figure 7. Analytical estimated flux density waveforms compared with the FEM simulations: (a) Teeth; (b) Yoke.

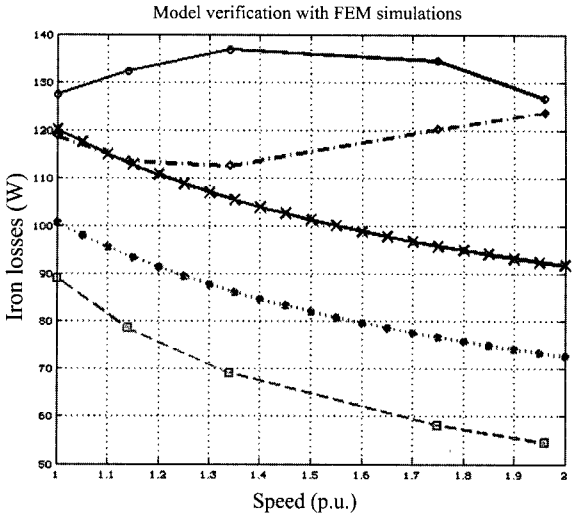

Figure 8. Model verification with the FEM simulations: [- ○ - FEM; - ◇ - Model II-trapezoidal; - □ - Model II-sinusoidal; - × - Model I-Deng; - ● - Model I-Mi].

can then be determined by using Equation (3) or more comprehensively as transient magnetic studies over one complete period:

$$P_{fe\_t}=\left\{\begin{array}{l}k_hB_t^2f+\left[\frac{1}{T}\int_0^T k_e\left(\frac{dB_t}{dt}(t)\right)^2\cdot dt\right]\\+\left[\frac{1}{T}\int_0^T k_{exc}\left(\frac{dB_t}{dt}(t)\right)^{3/2}\cdot dt\right]\end{array}\right\}\cdot V_t \tag{20}$$

$$P_{fe\_y}=\left\{\begin{array}{l}k_hB_y^2f+\left[\frac{1}{T}\int_0^T k_e\left(\frac{dB_y}{dt}(t)\right)^2\cdot dt\right]\\+\left[\frac{1}{T}\int_0^T k_{exc}\left(\frac{dB_y}{dt}(t)\right)^{3/2}\cdot dt\right]\end{array}\right\}\cdot V_y \tag{21}$$

5. COMPARISONS OF MODEL I AND MODEL II WITH FEM AND DISCUSSION

In this section, the analytical approaches, Model I and Model II, presented in this paper are applied to a design example of a four-pole PM synchronous motor for traction applications. The stator outside diameter is 188 mm and the machine active length is 165 mm. The continuous output power of the motor is about 3.2 kW.

A time-stepping FEM is also applied to the same design for the verification of the proposed analytical models. The computed losses at various speeds up to twice the rated speed from both models are compared

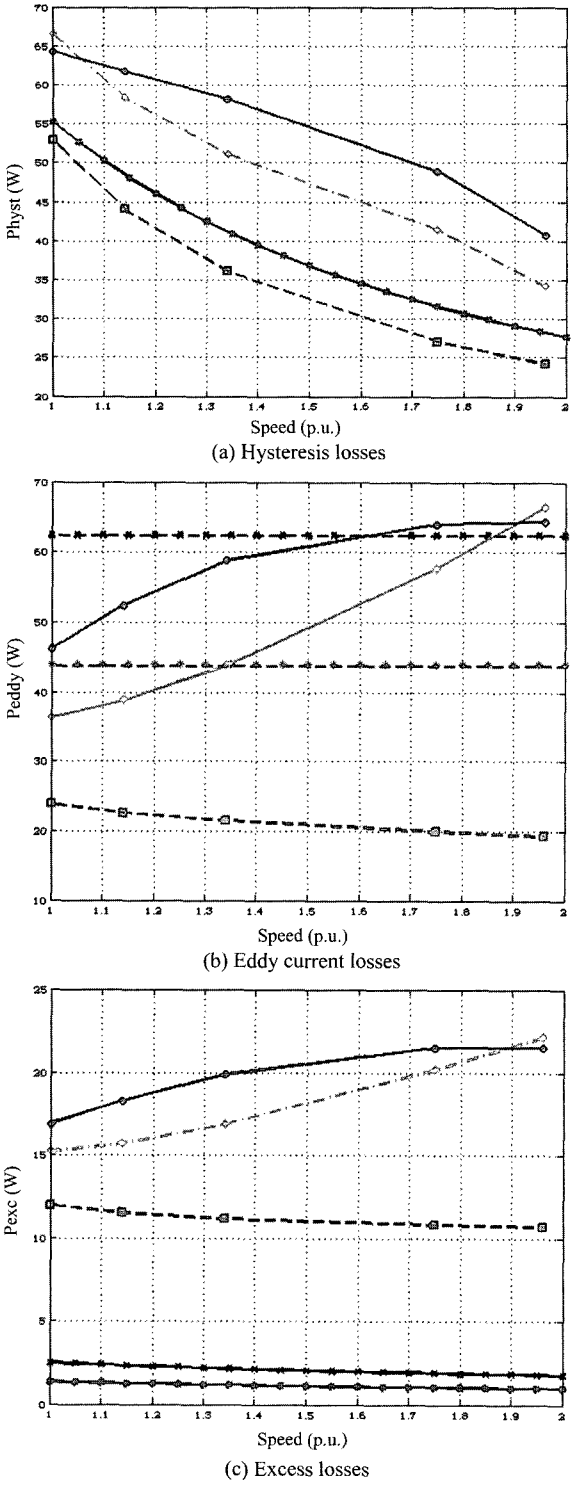

Figure 9. Iron loss component: (a) Hysteresis losses; (b) Eddy current losses; (c) Excess losses [- ∗ - FEM; - ◇ - Model II-trapezoidal; - □ - Model II-sinusoidal; - × - Model I-Deng; - ○ - Model I-Mi].

with the FEM results, as shown in Figure 8. In addition, Figure 9 shows a comparison of the different analytical model to the FEM results for each loss component.

From the results, Model II with trapezoidal approximation shows a most satisfactory agreement with the FEM simulations among all the proposed models. The difference is expected as the teeth and yoke analytical flux density waveforms are not perfectly matching with the results from FEM computations. Nevertheless, unlike the other proposed approaches in this study, the trend of the eddy current and excess losses increases as the speed increases provides a promising sign for further emendations. All the other models studied are proved to be rather inadequate for estimating the losses in the flux-weakening region. This is due to the fact that sinusoidal approximation is no longer valid to predict the phenomenon inside the motor, as the distortion of the flux density waveform is getting more and more pronounced when the speed increases. As a result, the significant harmonics losses from these distortions contribute to the increasing of the eddy current and excess losses. This consequently elucidates that an accurate flux density variation is essential for estimations of the iron losses, especially in the field-weakening region.

6. CONCLUSION

Two different analytical approaches for estimating the iron loss of a PM motor are presented and investigated. The results from these methods are compared with the FEM computations. From the results, it is concluded that only Model II with trapezoidal approximation shows a satisfactory trend of the losses at various speeds. To further evaluate the proposed models, results for a wide operating speed range will be compared with the test data of a prototype motor in the continuing phase of the study. It is also concluded that analytical approaches based on the pure sinusoidal waveform are not adequate for losses estimations in the field weakening operation due to the significant amount of harmonic iron losses.

ACKNOWLEDGEMENT–The authors would like to express their gratitude to Cedrat for the technical support in using FLUX2D.

REFERENCES

Berotti, G. *et al.* (1991). An Improved estimation of iron losses in rotation electrical machines. *IEEE Trans. on Magnetics* **27**, **6**, 5007–5009.

Deng, F. (1999). An Improved Iron Loss Estimation of Permanent Magnet Brushless Machines. *IEEE Trans.*

on Energy Conversion **14**, **4**, 1391–1395.

Gieras, J. F. and Wing, M. (2002). *Permanent Magnet Motor Technology.* 2nd edn. Marcel Dekker. New York.

Jamil, M. K. and Demerdash, N. A. (1990). Harmonics and core losses of permanent magnet DC motors controlled by chopper circuits. *IEEE Trans. on Energy Conversion* **5**, **2**, 408–414.

Levers, J. D., Biringer, P. P. and Hollitscher, H. (1978). A simple method of estimating the minor loop hysteresis loss in thin laminations. *IEEE Trans. on Magnetics* **14**, **5**, 386–388.

Mi, C., Slemon, G. R. and Togawa, N. (1984). Modelling of iron losses of surface mounted permanent magnet synchronous motors. *IEEE IAS Annual Meeting* **4**, 2585–2591.

Sagawa, M. (1984). New material for permanent magnets on a base of Nd and Fe. *Jour. Appl. Phys* **55**, **6**, 2083–2087.

Sebastian, T. and Slemon, G. R. (1987). Operating limits of inverter driven permanent magnet motor drives. *IEEE IAS Annual Meeting* **23**, **2**, 327–333.

Slemon, G. R. and Liu, X. (1990). Core losses in permanent magnet motors. *IEEE Trans. on Magnetics* **26**, **5**, 1653–1655.